King Saud University

Arabian Journal of Chemistry

www.ksu.edu.sa
www.sciencedirect.com

ORIGINAL ARTICLE

Ultra-fast sustainable synthesis, optimization and characterization of guava phenolic extract functionalized nanosilver with enhanced biomimetic attributes

Fredrick Nwude Eze [a,b,*], Chitchamai Ovatlarnporn [a,b,c,*],
Sirinporn Nalinbenjapun [a,b,c], Sasikarn Sripetthong [a,b,c]

[a] *Drug Delivery System Excellence Center, Prince of Songkla University, Hat Yai, Songkhla 90112, Thailand*
[b] *Faculty of Pharmaceutical Sciences, Prince of Songkla University, Hat Yai, Songkla 90112, Thailand*
[c] *Department of Pharmaceutical Chemistry, Faculty of Pharmaceutical Sciences, Prince of Songkla University, Hat Yai, Songkla 90112, Thailand*

Abstract   There had been some reports demonstrating the green synthesis of silver nanoparticles using guava (*Psidium guajava* (L.) extract); however, detailed and in-depth interrogation of the vital synthesis parameters for rapid, facile, efficacious synthesis at room temperature, and robust characterization of the as-prepared nanoparticle is currently lacking. This study presents a comprehensive delineation of the sustainable phyto-fabrication of biogenic guava phenolic extract functionalized silver nanoparticles (GVE-SNP) based on guava phenolic extract as the sole reductant/stabilizer, as well as the synthesis optimization, thorough physicochemical characterization and potential biological applications of the as-prepared nanosilver. The results revealed that successful synthesis of GVE-SNP was instantaneous and maximum intensity of the plasmonic peak at 425 nm was achieved in less than 10 min. GVE-SNP was found to present stable, well-dispersed, round, uniform, and crystalline nanoparticles of about 5.88 nm. The FTIR and RAMAN spectra indicated that GVE-SNP surface was properly capped by bioactives from GVE. The nanoparticles displayed potent radical scavenging activity against $ABTS^{·+}$ and $DPPH^{·}$. Also, GVE-SNP exhibited a

* Corresponding authors at: Faculty of Pharmaceutical Sciences, Prince of Songkhla University, Hat Yai, Songkhla 90112, Thailand (F.N. Eze), Department of Pharmaceutical Chemistry, Faculty of Pharmaceutical Sciences, Prince of Songkla University, Hat Yai, Songkla 90112, Thailand (C. Ovatlarnporn).
  E-mail addresses: fredrick.e@psu.ac.th (F.N. Eze), chitchamai.o@psu.ac.th (C. Ovatlarnporn).

ELSEVIER | **Production and hosting by Elsevier**

significant and dose–response inhibitory effect against tyrosinase. Furthermore, the nanoparticles displayed good cytotoxicity against L929 fibroblast and were found to possess strong antimicrobial properties, inhibiting the growth of *S. aureus* and *S. epidermidis*.

1. Introduction

Recently, there has been an unprecedented surge of interest in nano-materials due to their widespread applications. Nanomaterial have found application in food, agriculture, healthcare, medicine, environment, pharmaceutical and cosmeceutical industries. Because of the current high demand for nanomaterials with known and novel applications, there has been a consistent research effort towards the production of nanomaterials that are not only less-expensive, but also safe and eco-friendly.

In general, two approaches have been recognized for nanoparticle synthesis: top-down and bottom-up. The top-down synthesis approach consists of breaking down bulk materials by different physical and chemical treatments into nano-sized particles. The bottom-up approach in contrast, composes of the assembly of nanomaterials from the most basic constituents, i.e., atom to atom or molecule to molecule. While both approaches have their limitations and advantages, green synthesis which is a bottom-up approach is more sustainable, eco-friendly, cost-effective, free from chemical contaminants and generally safer (Jamkhande et al., 2019). Green synthesized silver and gold nanoparticles have been shown to possess diverse biologically, pharmaceutically and cosmeceutically relevant functionalities, including antimicrobial, antioxidant, antifungal, tyrosinase inhibitory, and UV radiation protective attributes (Eze and Nwabor, 2020; Singh et al., 2021). For example, silk sericin-based composites and hydrogels with *in situ* synthesized silver nanoparticles prepared via a green route were shown to exhibit remarkable antibacterial and wound healing properties (He et al., 2017; Tao et al., 2021, 2019a, 2019b). Similarly, plant-based synthesis of metal nanoparticles have grown in popularity owing to the many potential applications of the synthesized nanomaterials. Certainly, the biological and physico-chemical attributes of phyto-mediated biogenic nanoparticles are dependent on the phytoconstituents employed as reductants and/or stabilizers. Various plant extracts have so far been investigated for their efficacy and capacity to synthesize silver or gold nanoparticles with desirable attributes, such as for sensing (Detsri et al., 2018), detoxification (Eze et al., 2019), catalytic degradation of toxic organic dyes (Selvaraj et al., 2021; Varadavenkatesan et al., 2021, 2020), food packaging (Costa et al., 2012), as antimicrobials, antioxidants, antiaging agent (Eze and Nwabor, 2020), antidiabetics (Das et al., 2019), anti-inflammatory agent (Kedi et al., 2018), and whitening agent (Jiménez et al., 2018).

Psidium guajava (L.), widely known as guava tree is common in Africa, Asia, Eastern Europe and several other parts of the world. The plant is often cultivated for its succulent fruits, medicinal and ornamental values. Guava leaves are rich in bioactive ingredients such as phenolics, flavonoids, tannins, ascorbic acid, proteins and polysaccharides which can serve as effective reductants/stabilizers of metal nanoparticles. The high abundance and availability of guava leaves make it a cheap bioresource for the sustainable synthesis of metal nanoparticles. Indeed, this has attracted considerable interest with some investigators demonstrating the synthesis of silver nanoparticles using crude polysaccharides (Wang et al., 2017), flavonoids fraction (Wang et al., 2018a) and crude aqueous guava leaves extract (Wang et al., 2018b). Although the synthesis of nanosilver using plant constituents as reductants is quite simple, as evidenced in the growing reports on green synthesis, it is very important to underscore that achieving reproducible synthesis of high quality, stable, well-dispersed colloidal silver nanoparticles from phytoextracts is particularly challenging (Xia et al., 2009). This difficulty is partly associated

with the initially formed Ag^0 nuclei which then develops into mature nanoparticles of various crystal sizes and morphologies depending on the changes in reaction conditions such as reductants, stabilizers, concentrations, temperature, reaction time, and presence of other additives (Chernousova and Epple, 2013). The complex nature of most phytoextracts adds to this challenge.

Previous reports on the preparation of nanosilver using guava extract had been very sketchy, with most lacking vital details including the concentration of the reductant, optimization of synthesis parameters and thorough characterization of the prepared nanomaterial (Nguyen et al., 2020; Ntoumba et al., 2019; Sougandhi and Ramanaiah, 2020; Venugopal, 2017). This is worthy of note because the unique attributes of noble metal nanoparticles are not only influenced by their composition but also by their particle size, size distribution, crystallinity, morphology, surface functionalization as well as charges. Another major limitation is the longer duration required for efficacious synthesis, typically taking several hours (Nguyen et al., 2020; Ntoumba et al., 2019; Sougandhi and Ramanaiah, 2020) compared to chemical reduction with reagents such as sodium borohydride which often takes only a few minutes. In cases where the crude extracts were partially purified in a bid to expedite the synthesis, the extract preparation often involved the use of noxious organic solvents or tedious fractionation procedure with microporous resins (Wang et al., 2018a, 2017). These are very important considerations, especially for the large-scale and industrial production of biogenic nanosilver in a manner that is simple, fast, reproducible, scalable, commercially viable as well as health- and eco-friendly. An Ag nanoparticle preparation approach that can satisfy these requirements is rare at this moment.

With a multitude of reducing equivalents and bulky chemical moieties, bio-phenolics have demonstrate remarkable efficiency as simultaneous reductants and stabilizers in biogenic production of nanosilver (Bhutto et al., 2018). Given its high phenolic content, guava leaf is an ideal candidate for the production of bio-phenolic-rich extract. Thus, the current work aimed at the fabrication and characterization of biomimetic silver nanoparticles in a simple, fast and truly sustainable manner based on guava leaf phenolic extract for various biological applications. The guava phenolic extract would serve as the sole reductant and capping agent and would equally be prepared using a facile green approach. To the best of our knowledge, the current investigation describes the most comprehensive report on the synthesis, optimization, and characterization of guava extract mediated biogenic nanosilver. Also, the biological attributes of the as-prepared nanoparticle would be well elucidated.

2. Materials and methods

2.1. Preparation of phenolic-rich guava extract (GVE)

Guava leaves was obtained locally in Songkhla province, Thailand. The identity of the plant sample was authenticated by matching with a reference sample (voucher specimen number: SKP 123 160701) domiciled at the Herbarium of the Faculty of Pharmaceutical Sciences, Prince of Songkla University, Thailand. The powder (60 g) was extracted with 1600 mL of 70% ethanol (v/v) using an overhead electric stirrer at 300 rpm for 2 h. The extract was filtered, and the filtrate was re-extracted using 1600 mL of fresh solvent. Both filtrate were

combined, and ethanol was evaporated under reduced pressure. The aqueous extract was freeze-dried to give a light brown phenolic-rich powder (GVE).

2.2. Determination of total phenolic content

The amount of phenolic constituents in the extract was assessed using Folin-Ciocalteu assay as previously described (Eze et al., 2019). The standard curve was prepared using gallic acid and the total phenolic content was expressed in mg gallic acid equivalent per gram of GVE in dry weight (mg GAE/g GVE dw).

2.3. Synthesis of biogenic silver nanoparticles

Biogenic silver nanoparticles was synthesized as previously described (Jayeoye et al., 2021). Briefly, into 95 mL of aqueous silver nitrate (0.5–2 mM) being stirred on magnetic stirrer was added 5 mL of guava extract (5 mg/mL) solution. Prior to addition, the pH of the extract was adjusted to 9.0. The reaction mixture was monitored visually and through UV–visible spectroscopy for 2 h.

2.4. Characterization of GVE-SNP

UV–vis analysis was performed as previously described (Eze et al., 2019). The UV–vis spectrum of the extract and the as-synthesized GVE-SNP was monitored at room temperature using UV–visible spectrophotometer (Agilent Technologies, Cary 60, USA). The unique surface plasmon resonance band characteristic of oscillating silver nanoparticles was also noted. The shape and distribution of the as-prepared silver nanoparticles was evaluated using transmission electron microscopy. The as-prepared nanoparticles was diluted with ultrapure water (1:150 v/v). A drop of the diluted nanoparticles was carefully placed on the TEM grid and air-dried at room temperature. The nanoparticles was observed using electron microscope, JEM-2010 (JEOL ltd., Tokyo, Japan) operating at 160 kV. The surface morphology of the nanoparticles was examined using field emission scanning electron microscopy (FESEM), Apreo, FEI (Czech Republic). FTIR analysis of the obtained nanoparticles was performed on Perkin Elmer (USA) Spectrum FTIR spectrometer and 32 scans were obtained per sample at a resolution of 4 cm^{-1}. The RAMAN spectra of the nanoparticles was obtained using Raman Microscope Spectrometer, RAMANforce, Nanophoton, Japan at an excitation wavelength of 532.06 nm, power of 0.10 mW, power density of 2.72×10^3, and wavelength range of 0–4000 cm^{-1}. X-ray diffraction spectra of the samples were obtained using X-ray diffractometer, Empyrean, PANalytical (Netherlands) operating at 40 kV and 30 mA, with Cu Kα radiation at a wavelength of 0.154 nm over a scan range (2θ) of 5 to 90° at s at a speed of 70.2 s. Additionally, the hydrodynamic diameter and zeta potential of the nanoparticles were recorded using Zetasizer Nano ZS (Malvern Instruments, Worcestershire, UK). The resistance of the nanoparticle to thermal degradation was evaluated using thermogravimetric (TGA) analysis. TGA analysis of the sample was performed on Thermogravimetric Analyzer, TGA8000 (Perkin Elmer, USA) with a scanning program consisting of heating from 25 °C to 800 °C at 5 °C/min under an atmosphere of nitrogen.

2.5. Antioxidant properties

2.5.1. DPPH (2, 2, - diphenyl-1-picrylhydrazyl) radical scavenging assay

GVE, GVE-SNP and Vit C solution (120 μL) were separately added into different wells of a 96-well microplate. DPPH solution (0.1 mM, 120 μL) was subsequently added to the samples and incubated for 30 min in the dark at room temperature. The absorbance of the solutions were recorded at 515 nm and the anti-radical activity was expressed as percentage inhibition (Das et al., 2019).

2.5.2. ABTS assay

ABTS reagent was prepared by mixing equal volumes of ABTS and potassium persulfate solution followed by incubation for 12 to 16 h. The working solution was prepared by diluting the stock solution to an OD of 0.70 ± 0.01 at 730 nm. GVE, GVE-SNP and Vit. C (15 μL) were added separately to ABTS reagent (180 μL) in the plate and incubated for 10 min. The absorbance of the solutions were recorded at 730 nm and the anti-radical activity calculated as percent inhibition (Das et al., 2019).

2.6. Tyrosinase inhibitory activity

Tyrosinase inhibitory activity of the samples was determined as described previously (Jiménez et al., 2018). Phosphate buffer solution (120 μL, 20 mM, pH 6.8) was added into 96-well plate. L-DOPA solution (5.07 mM, 20 μL) was added into the plate followed by 20 μL of GVE (90 μg/mL), GVE-SNP (90 μg/mL) or Kojic acid (45 μg/mL). The solutions were incubated in the dark for 5 min. Subsequently, 20 μL of tyrosinase (500 units/mL) was added to the mixtures and incubated for 20 min. The absorbance of the mixtures was read at 475 nm. The tyrosinase inhibitory activity was expressed as percentage inhibition.

2.7. Antimicrobial activity

The antimicrobial properties of GVE-SNP against selected gram positive bacterial isolates was evaluated using agar well diffusion assay as previously described (Eze et al., 2019). GVE and media solution served as controls, while vancomycin was used as the positive control.

2.8. Determination of cell viability by MTT assay

The cytotoxic effect of the nanoparticles was assessed on mouse L929 fibroblast using MTT assay as previously described (Eze et al., 2021). Briefly, cultured cells in 96-well plates (1.5×10^4/well) were challenged with various concentrations of GVE-SNP in culture media. Cells treated with only culture media served as control. The plate was subsequently incubated for 24 h. Thereafter, the viability of the cells were determined using MTT assay.

3. Results and discussion

3.1. Preparation of phenolic-rich guava extract

It is well-known that the efficacy of phyto-mediated biogenic synthesis of metal nanoparticles is a function of the type and

content of phytoconstituents acting as reductants and/or stabilizers (Bhutto et al., 2018). Plant phenolic-rich extracts had previously been demonstrated as efficacious reducers/stabilizers of gold and silver nanoparticles (Nath et al., 2020). In this work, phenolic-rich extract from guava leaf was prepared in a facile and eco-friendly approach that did not require any toxic organic reagent. The approach gave a high yield of 18% (w/w) phenolic-rich guava extract as a light brown hydrophilic powder. The total phenolic content was 96.85 ± 1.76 mg GAE/g GVE dw. Several authors had previously noted the high content of phenolics in guava leaf (Rahman et al., 2018). Besides, the current approach had been demonstrated to recover high yields of phenolics (Eze et al., 2019). In light of the above, the obtained extract is expected to be rich in phenolic constituents present in guava leaf, such as quercetin, gallic acid, guaijavarin, catechin, epicatechin, rutin, gallic acid, kaempferol and glycosides (Lorena et al., 2022; vBarbalho et al., 2012; Rahman et al., 2018). It is germane to underscore that the approach used to prepare GVE is very simple, but more importantly, no toxic organic solvent or residue was needed or created. This was clearly different from previous works where conventional noxious organic solvents such hexane or dichloromethane were used for removing chlorophyll and other lipophilic pigments from the extract. The high total phenolic compounds of GVE was a good indicator of its potential for efficacious synthesis of biogenic silver nanoparticles.

3.2. Preparation and characterization of biogenic silver nanoparticles (GVE-SNP)

Successful synthesis of biogenic silver nanoparticles based on GVE monitored visually and using UV–vis spectroscopy (Fig. 1). Upon addition of GVE solution to silver nitrate solution, the clear colorless Ag solution instantly became sparkling yellow suggesting the formation of silver nanoparticles. Notably, there was a concentration dependent increase in the color intensity of the solutions in relation to the concentration of silver nitrate (Fig. 1A). Concurrently, the UV–visible spectra of the nanoparticle solutions were obtained from 280 to 700 nm (Fig. 1B). The ostensible presence of an absorption maximum around 425 nm was because of the surface plasmon resonance (SPR) band of oscillating nanoparticles due to the incident light, and a strong indication of the presence of silver nanoparticles in the solution. The nanoparticle solutions featured prominent SPR peaks at 418, 425, 431, 430/31 nm for 0.5, 1, 2, and 4 mM of AgNO$_3$ solutions. It is generally accepted that there is a direct relationship between the λ^{max} and the size of the obtained nanoparticles (Navarro and Werts, 2012; Paramelle et al., 2014). As such, the solution prepared with 0.5 mM AgNO$_3$ will feature nanoparticles with the smallest size. On the other hand, the SNP solution from 4 mM AgNO$_3$ did not only present a lower λ^{max} intensity, but also seem to aggregate. Also, judging from the intensities of the UV–vis spectra, the highest intensity was recorded for the solution with 1 mM AgNO$_3$. Thus, based on the λ^{max} and intensity, 1 mM AgNO$_3$ was used as the optimal metal salt concentration. Similar to metal salt concentration, the synthesis was optimized for time by monitoring the λ^{max} at 425 nm from 0 to 60 min (Fig. 1C). Indeed, it appeared that there was no major change in both the intensity and peak position of the reaction solution from 0.5 to 60 min, underscoring the instant

reduction of the precursor into nanosilver. The relationship between the synthesis and time was further depicted in a curve to understand the kinetics (Fig. 1D). During this timeframe, the highest absorbance was recorded between 7.5 and 10 min. Beyond 10 min, the absorbance seemed to decline slightly (Fig. 1D). The impact of pH on the synthesis effectiveness was equally assessed. The pH of GVE solution was quickly adjusted before adding to the solution of AgNO$_3$. The UV–visible spectra and corresponding image of the as prepared GVE-SNP various pH conditions is presented in Supplementary Fig. S1. In general, a pH-dependent increase in the intensity of the UV–vis spectra of GVE-SNP solutions can be seen. At slightly acidic pH 5.5, no clear SPR band was seen. However, as the pH increased, i.e., $6.5 - 8.6$, not only did a prominent SPR band appeared around 425 nm, with sharp and symmetrical peaks, but the peak intensities also increased correspondingly. Similar, the intensity of the characteristic yellow color of the nanoparticle solution deepened. Polyphenolic compounds such as guaijavarin and quercetin which populate GVE are more soluble and tend to autoxidize at alkaline pH (Jurasekova et al., 2014). Under this condition hydrogen atoms are made available for the bioreduction of silver ions (Ag$^+$) into nanosilver (Ag^0). This perhaps explains the rapid and efficacious synthesis at pH 8.6. It is also worth mentioning that phenolic compounds tend to easily degrade at very high pH, reducing their capacity not only as reductants but also as stabilizing agents of the as-formed nanoparticles (Jurasekova et al., 2014). Very high pH ≥ 10 was excluded in this work since this has been shown to undermine nanoparticle stability and instead favor aggregation (Brasiunas et al., 2021). Therefore, for reproducible guava phenolic extract mediated synthesis of biogenic SNP, the optimized condition consisted of final concentration of extract and silver precursor of 0.25 mg/mL and 0.169 mg/mL, respectively, at room temperature and pH 8.6 for 10 min.

The phyto-fabrication of silver nanoparticles can be broadly elucidated in three stages: reduction, growth and stabilization (Jayeoye et al., 2021). During the reduction and nucleation phase, silver ions (Ag$^+$) in the silver nitrate solution are autocatalytically reduced by polyphenols and powerful flavonoids in GVE, such as quercetin and guaijavarin into small sized silver nanoparticles (Ag^0). During the growth phase, excess Ag$^+$ ions in the solution react with bioactives on the surface of the formed small-sized silver nanoparticles, become reduced, leading to the formation of large-sized silver nanoparticles (Thanh et al., 2014). In the stabilization phase, the mature silver nanoparticles are stabilized in solution by polyphenols and other compounds including sugars, so as to ensure that the particles are well-dispersed and free from aggregation or precipitation. For instance, the carboxylic groups of gallic acid present in GVE are capable of covering the surface of the as-formed SNP by electrostatic attraction (Lorena et al., 2022; Yoosaf et al., 2007). Given that the surface of every SNP in the solution is now covered by these relatively large compounds, they tend to be more stable (Iravani et al., 2014). Moreover, since the surrounding groups on the surface of the individual SNP have the same kind of charges, they tend to repel each other, thereby ensuring that the nanoparticles stay freely dispersed in the solution. Schematic depiction of the putative synthesis mechanism of GVE-SNP is presented in Fig. 2.
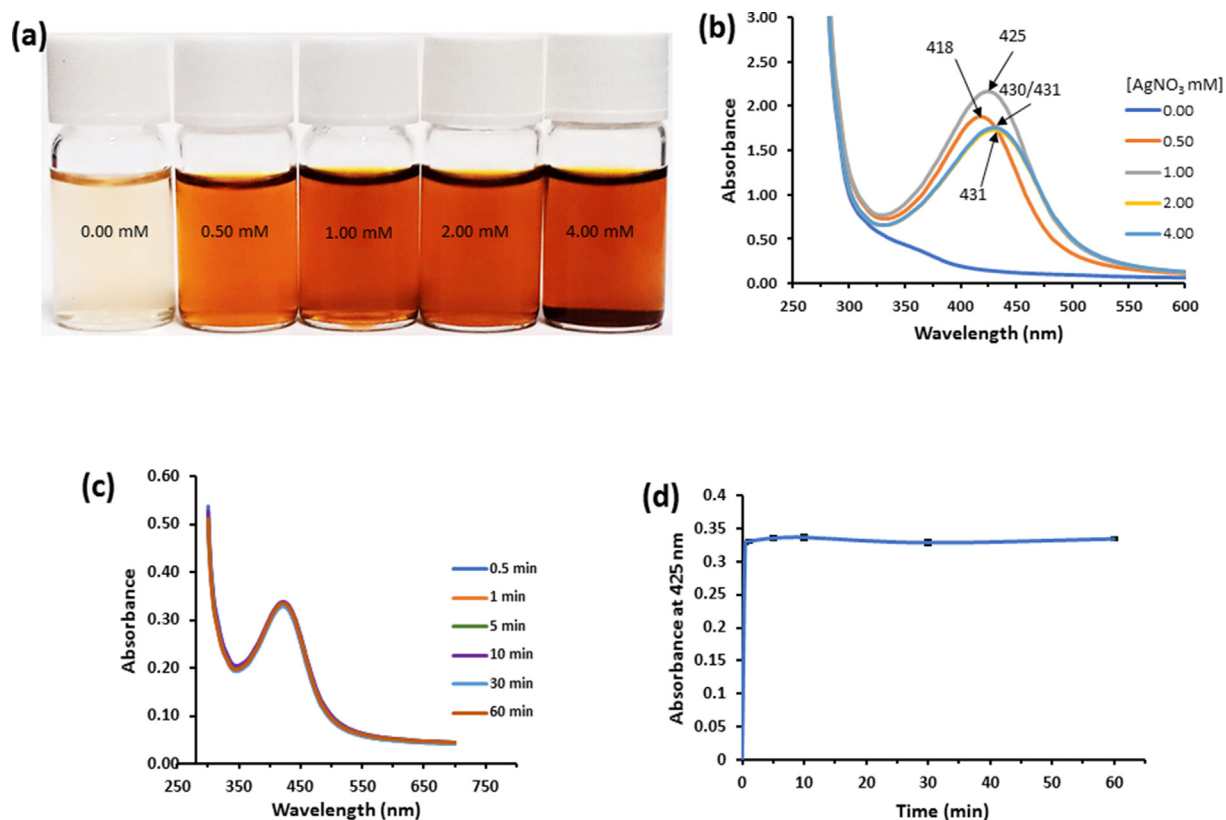
Fig. 1 (a) Photographic representation of GVE-SNP solution synthesized with increasing concentrations of AgNO$_3$. (b) Corresponding UV–visible spectra of the as-synthesized GVE-SNP. (c) Effect of time on GVE-SNP synthesis. (d). Plot of absorbance at 425 nm against time for the synthesis of GVE-SNP using 1 mM AgNO$_3$ solution at room temperature.

Given that the biological and physico-chemical properties of metal nanoparticles are often dependent on their size and shape, the morphology of GVE-SNP was evaluated using TEM. The electron micrograph revealed that the as-synthesized GVE-SNP were round and well-dispersed (Fig. 3A). The high resolution TEM image (Supplementary Fig. S2) and concentric rings revealed in the selected area electron diffraction (SAED) pattern (Fig. 3D) indicated that the nanoparticles are of pure crystalline nature. The observed bright white rings apparently emerged from reflections of the
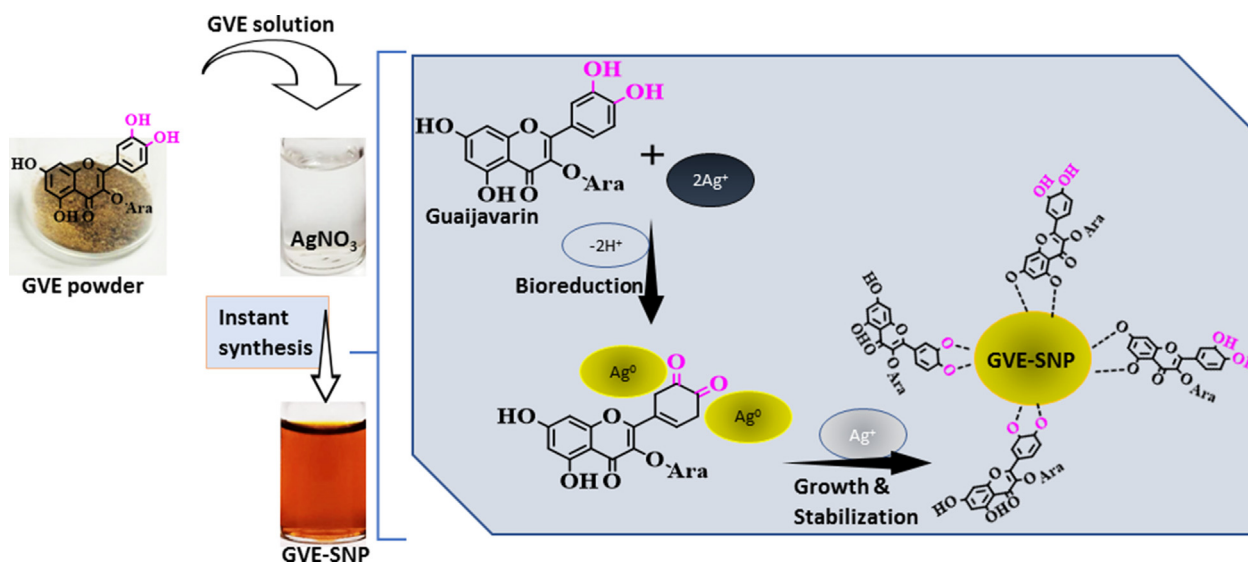

Fig. 2 Schematic representation of putative mechanism of synthesis for GVE-SNP from guava phenolic extract as the reductant/stabilizer and silver nitrate solution as the precursor.
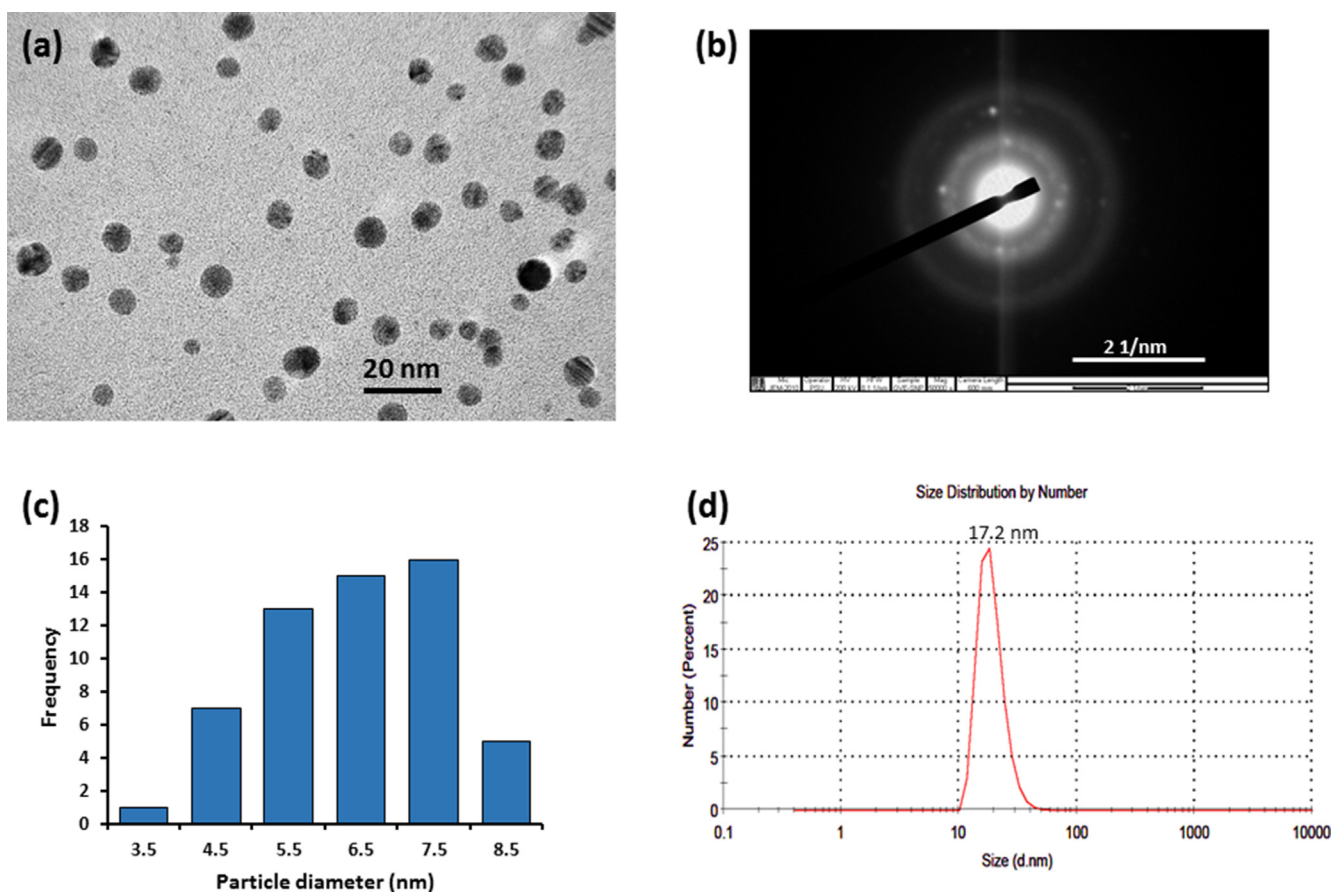
Fig. 3 (a) TEM micrograph of GVE-SNP obtained at 250,000 x. (b) Selected area electron diffraction (SAED) pattern (c) Particle size distribution of GVE-SNP captured by TEM and prepared with ImageJ software and (d) Hydrodynamic particle size distribution obtained by DLS.

Bragg's planes of *fcc* silver. The particle size analysis of the nanoparticles based on the TEM micrograph using ImageJ software revealed that GVE-SNP had a mean particle diameter of about 5.88 nm. The nanoparticles presented a relatively narrow distribution with over 70% of the sample having a diameter in the range 4.4 to 7.5 nm (Fig. 3C). Furthermore, the size of the nanosilver in aqueous solution was also determined by DLS. The DLS technique in principle measures the random motion of the particles due to bombardment by surrounding fluid (Brownian motion) and relates this to particles size. It is important to mention that the velocity of the Brownian motion is defined by an entity known as the translational diffusion coefficient and the size of the particles is calculated from this property using the Stokes-Einstein equation. Given that the diameter that is obtained via DLS is a value that indicates how a particle diffuses within a fluid, this diameter is referred to as the hydrodynamic diameter. This diameter is that of a sphere of equivalent translational diffusion coefficient. The translational diffusion coefficient is dependent on the particle 'core', any surface structure, as well as the type and concentration of ions in the fluid. Consequently, the DLS is capable of providing complementary information with regards to the interaction behavior of the nanoparticles with the surrounding milieu (Ruseva et al., 2018). Herein, the colloidal nanosilver had an average hydrodynamic size of 17.2 nm (Fig. 3D), which was larger than the TEM data. This apparent increase in the

DLS size data over that of TEM stems could be due to the fact that TEM measures the size of the dry particles on the grid whereas the DLS value is a reflection of the hydrodynamic size of the nanoparticles, which is inclusive of the hydration shells around them (Gubitosa et al., 2020; Thomä et al., 2019). The phytochemicals on the surface of the nanoparticles also contributed to the hydrodynamic size. The poly dispersity index (PDI) of the colloidal nanoparticles obtained by DLS was 0.279. The PDI is a measure of the width of particle size distribution. The PDI value could vary from 0.0 (for a sample with perfect size uniformity) to 1.0 (highly polydisperse sample). Previously, Costa asserted that PDI values of 0.08–0.7 are typical for a system with average polydispersity (Costa, 2012) while Cervantes et al noted that particles with PDI values around 0.3 are adequate for cellular uptake (Cervantes et al., 2019). Based on the PDI value obtained for colloidal GVE-SNP solution, the sample of nanoparticles had acceptable size uniformity. Zeta potential measurement of the particles revealed a value of −24.69 mV, suggesting that the colloids were reasonably well-dispersed and stable in aqueous solution. The FESEM image portrayed small white specks against a dark background (Fig. 4A). The shiny white speckles represent the round shaped tiny silver nanostructures, which were found to be lower than 10 nm. EDX analysis revealed a substantial proportion of the nanomaterial was derived from silver (Fig. 4B). The presence of silver was revealed in the EDX

spectrum between 2.5 and 3.5 keV consistent with previous reports (Raghunandan et al., 2011). Other elements, notably, C, O, and Cl were also present, presumably from the bioactive compounds in GVE, which served as capping agents on the nanomaterial surface. The unassigned peak that emerged around 0.9 keV is likely from the brass stub where the GVE-SNP sample was mounted during the analysis. The elemental map of GVE-SNP indicated a uniform distribution of the silver in the nanostructure (Fig. 4C).

FTIR analysis was used to elucidate the functional group interactions that participated in the production of the nanoparticle. The infra-red spectrum of GVE revealed prominent absorption bands at 3369 cm^{-1} and 2928 cm^{-1} corresponding to the —O—H and C—H or N—H stretching vibrations, respectively (Fig. 5A). Other notable peaks were also observed at 1692 cm^{-1} (C═O stretching) and 1609 cm^{-1} (C═C stretching) and 1044 cm^{-1} (—C—O—C-stretching) (Qiao et al., 2014). The FTIR pattern of the nanoparticles was quite similar to that of the extract, suggestive of the presence of GVE metabolites on the surface of the nanostructure. Nonetheless, when both spectra were compared, some changes were observed in terms of the major peak positions. In particular, minor shifts were observed in most of the major peak positions appearing in GVE-SNP. For instance, the peaks at 1692, 1609, 1447 and 1210 cm^{-1} in GVE shifted to lower positions at 1691, 1603, 1442 and 1205 cm^{-1}, respectively in GVE-SNP, while the one at 1518 cm^{-1} moved to a higher wavenumber, 1523 cm^{-1}. What these peak transitions demonstrate are molecular interactions

between the components of GVE and the surface of the nano-material (Zhao et al., 2010), putatively contributing to its stability post-synthesis. The functional moieties deposited on the silver nanoparticles were further investigated using RAMAN spectrometry with the RAMAN spectra of the extract and nanoparticles presented in Fig. 5B. The extract exhibited weak RAMAN signals at 122, 1045, 1374 and 1531 cm^{-1}. The silver nanoparticles produced enhanced signals around the same locations at 117, 1063, 1352.6, and 1547 cm^{-1}, which were consistent with RAMAN shifts of polyphenolic compounds such as quercetin and ellagic acid derivatives (R. Pompeu et al., 2018). These compound had been noted as some of the major bioactives known to constitute guava extract (Díaz-de-Cerio et al., 2016). The sharp RAMAN peak at 236 cm^{-1} is indicative of the lattice vibration of Ag nanoparticles. Similar signal was previously observed at 233 cm^{-1} in the RAMAN spectrum of biogenic Ag nanoparticles from Neem extract (Ulaeto et al., 2020). The slight shift in peak positions of GVE-SNP relative to GVE can be attributed to intermolecular interactions between the bioactives and metal surface. The RAMAN profile of GVE-SNP confirmed that the surface of the metal nanoparticles was covered by bioactives from GVE. These findings are well corroborated by previous reports (Padilla-Cruz et al., 2021).

The crystalline attributes of the as-prepared GVE-SNP was characterized by X-ray diffraction analysis. Peaks of the diffractogram were observed at 2θ position 27–85° (Fig. 5C). Although the presence of some crystalline matter can be observed from the XRD profile of GVE, the plant extract
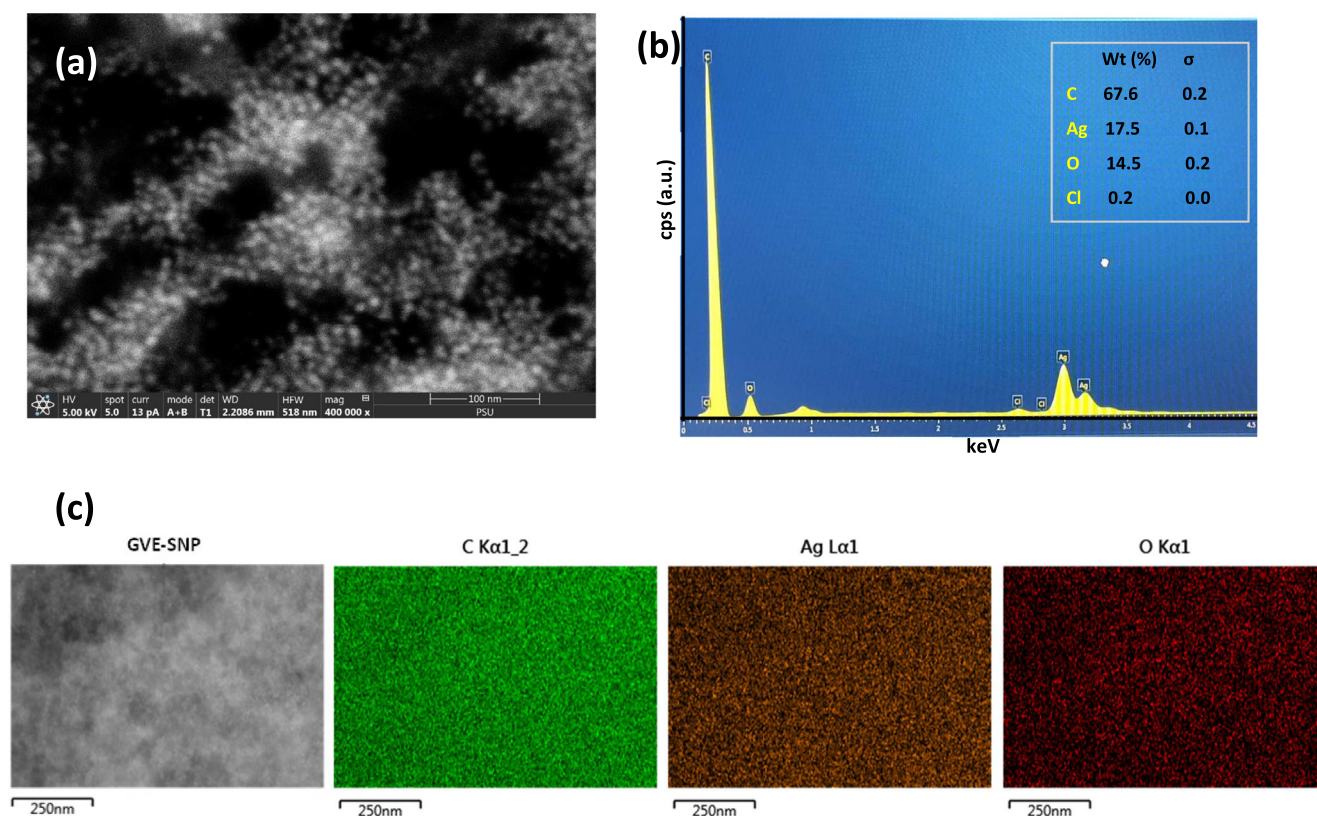

Fig. 4 (a) FESEM images GVE-SNP revealing the small nanoparticles as shiny white speckles (b) EDX spectra of GVE-SNP depicting strong peaks of silver between 2.5 and 3.5 keV and (c) Elemental maps of the different elements present in GVE-SNP revealing the uniform showing the uniform distribution of silver.
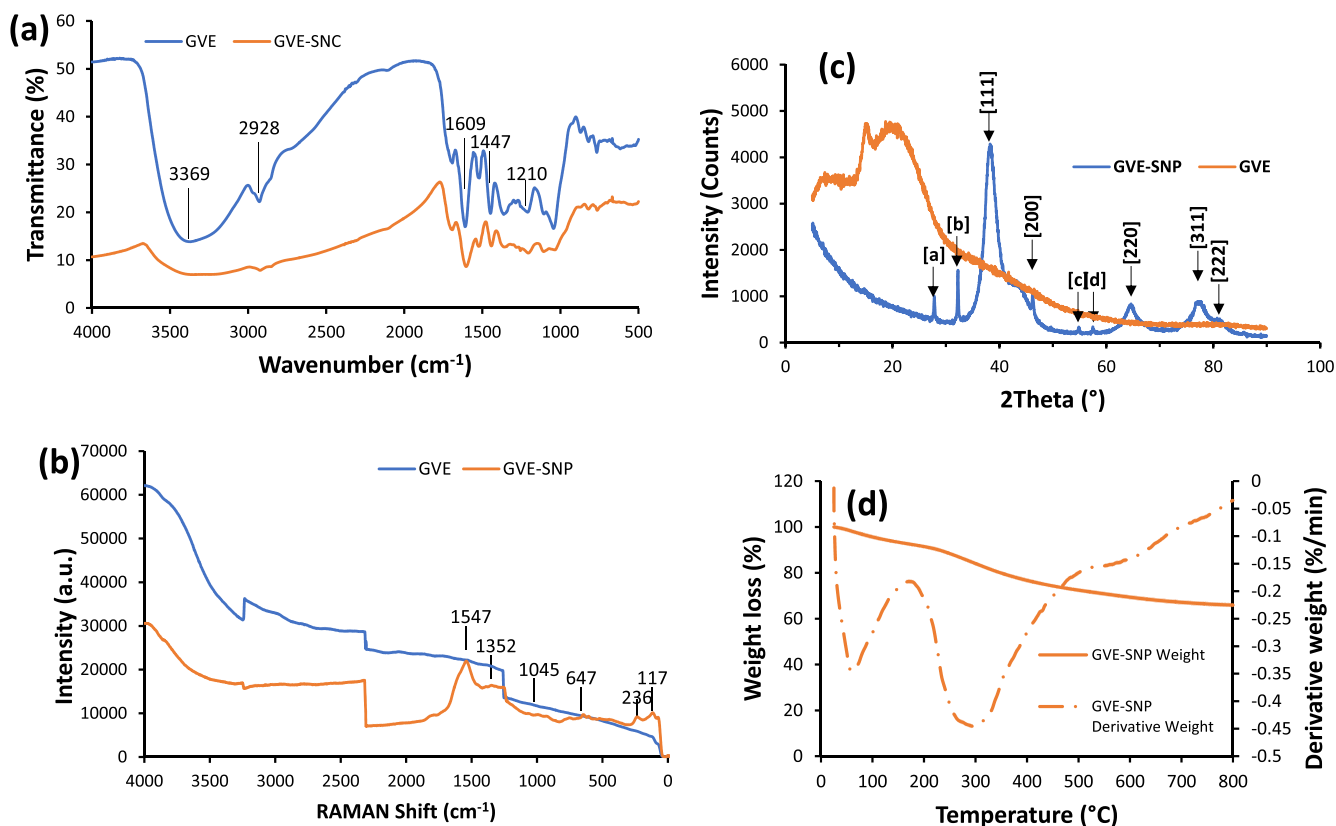
Fig. 5 (a) FTIR and (b) RAMAN spectra of GVE-SNP with peaks representative of major functional groups present in the nanomaterial. (c) XRD profile of GVE-SNP showing major diffraction peaks. (d) TGA/DTG thermograms of GVE-SNP.

was largely amorphous. Conversely, the XRD pattern of the nanostructure presented several clearly defined peaks. Of prominence were the peaks identified at 2θ (°) position around 38, 44, 64, 77 and 81, which corresponded to Bragg reflection of the (111), (200), (220), (311), and (222) crystallographic plane lattice. These can be attributed to the face centered cubic (fcc) crystal nature of the silver (ICDD No. 01-071-4613). Meanwhile, some minor peaks were also apparent in the XRD profile of GVE-SNP, such as those featuring at 2θ position 27.83° (a), 32.24° (b), 54.85° (c) and 57.48° (d). These peaks could be ascribed to the (111), (200), (311), (222) reflections of fcc of silver chloride crystallites (ICDD No. 00-031-1238) (Supplementary Fig. S3). The crystallite particle size of GVE-SNP was determined based on Scherrer's equation with peak position (2θ) at 38.26° given that it featured the maximum intensity. On the basis of its XRD data, GVE-SNP was found to have an average crystallite size of 4.56 nm. The d-spacing and hkl values were 2.3521 Å and (111), respectively. Upon computation, lattice parameter (a) of 4.0739 Å was obtained, which is consistent with the standard lattice parameter of silver, 4.0729 Å (Vinayagam et al., 2018).

The thermal stability of GVE-SNP was interrogated via thermogravimetric analysis. The TGA and DTG profiles of the nanoparticle is presented in Fig. 5D. The weight loss response of GVE-SNP as a function of increasing temperature can be characterized in three phases (Supplementary Table S1). The first phase spanning about 24–172 °C with an onset degradation temperature of 31.75 °C mainly reflects the loss of

bound water from the nanomaterial. The second phase found within the range of 172–518 °C represents the loss of volatile constituents, degradation and pyrolysis of organic components encapsulating the nanoparticle. Following the third stage of thermal degradation, the nanomaterial lost about 34% of its mass. Of particular significance was the considerable amount of residual ash at the end of the thermal procedure. This is noteworthy because the residual ash content can be taken as an approximation of the resistance of a material to thermal degradation. Compared to prior reports, the ash content of 65.94% is quite high and thus a strong indication of the superior thermal stability of GVE-SNP. This high thermal stability could be attributed to the strong binding of the capping agents over the surface of the nanoparticles. Encouraged by impressive physico-chemical attributes in terms of size, uniform morphology and distribution, as well as stability, we were prompted to evaluate the biological properties of GVE-SNP.

3.3. Biological characterization of GVE-SNP

3.3.1. Antioxidant activities of GVE-SNP

Nanomaterials have been shown to have antioxidant properties leading to the term 'Nanoantioxidants' (Sandhir et al., 2015). Interestingly, some of these nanomaterials even exhibited better antioxidant properties than their respective synthesis components (Rehana et al., 2017). In an attempt to know whether GVE-SNP possess any antioxidant property, ABTS and DPPH assays were performed. Generally, all the samples (GVE, GVE-SNP and Vit. C) demonstrated anti-radical activ-

ities on ABTS$^{\cdot+}$ and DPPH$^{\cdot}$ (Fig. 6). GVE-SNP exhibited potent anti-radical effect against ABTS$^{\cdot+}$ in a concentration dependent manner. Expectedly, vit. C, the standard, had the best antiradical activity of all the samples. What was even more notable was that GVE-SNP displayed better radical scavenging effect than GVE. It has been reported that AgNO$_3$ solution has no antioxidant activity. On the other hand, GVE is reputed for its strong antioxidant effect. The superior anti-radical activity of GVE-SNP could thus be an attribute of its features as a nanomaterial as well as the synergistic effect of the SNP and the GVE that covers its surface. Similar increase in the antioxidant property of plant mediated silver nanoparticles over the reducing/stabilizing plant extract had previously been reported for *Cassia fistula* extract (Eze et al., 2021).

3.3.2. Tyrosinase inhibitory activity of GVE-SNP

The synthesis and distribution of melanin, melanogenesis, takes place in specialized pigment producing cells (melanocytes) located amongst the basal layer epidermal cells and dermal macrophages of the skin. Melanin is the pigment responsible for skin complexion and, plays a vital role in protection of the skin against deleterious solar radiation which could lead to cancers and other diseases. However, excessive production of melanin could give rise to hyperpigmentation and skin discoloration. Melanin is synthesized in a cascade known as melanogenesis. Melanogenesis is largely a non-enzymatic oxidative process. The only enzyme involved in the production of melanin is tyrosine (Sugumaran and Barek, 2016). Thus, the inhibition of tyrosinase has been proposed as an effective approach for modulating the synthesis of melanin.

In this work, the tyrosinase inhibitory property of GVE-SNP was determined using the dopachrome assay. In the presence of the inhibitor, the enzymatic oxidation of L-DOPA into a brown solution is prevented. GVE, GVE-SNP and the standard kojic acid (KA) all inhibited tyrosinase (Fig. 7) and thus prevented the enzymatic oxidation of L-DOPA to dopaquinone. The suppression of tyrosinase activity by GVE-SNP was significant ($p < 0.001$) and occurred in a dose-dependent manner. Compared to both GVE and KA, the tyrosinase inhibitory effect of GVE-SNP was lower. It has been previously reported that guava leaf extract is a potent

inhibitor of tyrosinase (You et al., 2011). Thus, it is possible that the tyrosinase inhibitory effect of GVE-SNP is a product of the anti-tyrosinase property of the extract components that encapsulate the nanoparticles. This findings indicated that besides the remarkable antioxidant properties of GVE-SNP, the nanoparticles could also protect against melanin-induced hyperpigmentation and skin discoloration.

3.3.3. Cytotoxicity of GVE-SNP

The potential of GVE-SNP to impact normal cells was assessed using L929 fibroblasts derived from mouse connective tissue. L929 cells were selected considering their high sensitivity and wide used in *in vitro* toxicity testing. Untreated cells containing only the media was used as controls. The viability of L929 cells upon exposure of various concentrations of GVE-SNP is presented in Fig. 8A. The cells showed a high level of viability above 80% following 24 h incubation with GVE-SNP up to a concentration of 25 µg/mL. At GVE-SNP concentrations greater than 25 µg/mL, the cell viability reduced substantially to below 50%. These results indicated that the maximum non-cytotoxic concentration of GVE-SNP in L929 fibroblasts is 25 µg/mL. This concentration was taken into consideration in subsequent biological investigations.

3.3.4. Antimicrobial activity of GVE-SNG

The antimicrobial activity of GVE-SNP was investigated against the *S. epidermidis* and *S. aureus*. These Gram positive microbes have been implicated in wound infections, sinus infections, boils, endocarditis as well as other forms of inflammations. GVE-SNP was found to demonstrate inhibitory activities against the growth of these pathogens. The nanoparticles displayed inhibitory zones of 15.33 and 17.33 mm against *S. aureus* and *S. epidermidis* (Fig. 8B and C). At similar concentrations (23 µg), the hydrophilic extract did not show any inhibitory activity (Supplementary Fig. S4). Investigations by Biswas et al. previously noted that while some extracts of *P. guajava* pose modest antimicrobial activities, the aqueous extract was found to have no inhibitory effect on all the tested microbes including *S. aureus* (Biswas et al., 2013). Our finding are in accord with these previous reports. Against this backdrop, the antimicrobial activity of GVE-SNP could mainly
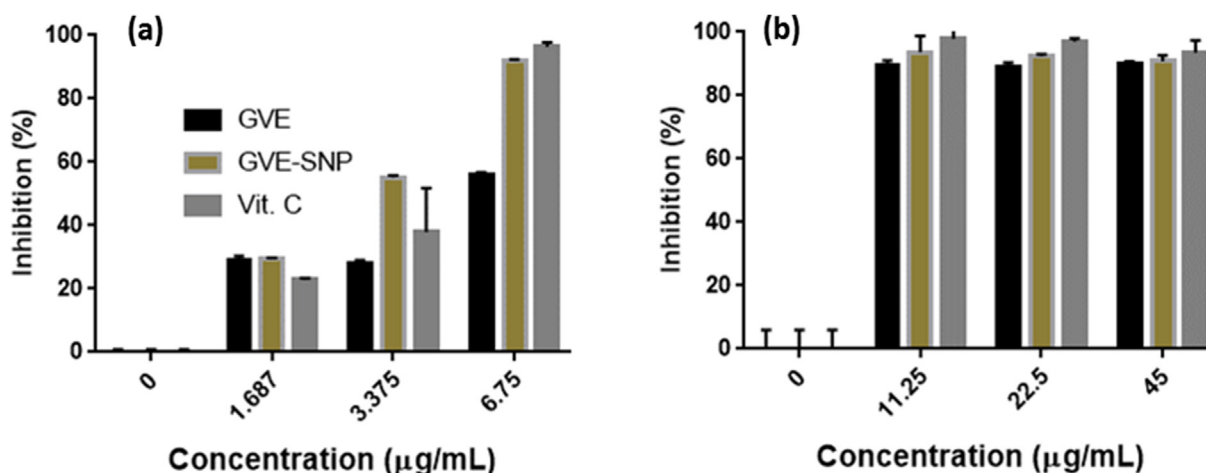

Fig. 6 Anti-radical activity of GVE-SNP against (a) ABTS$^{\cdot+}$ and (b) DPPH$^{\cdot}$.
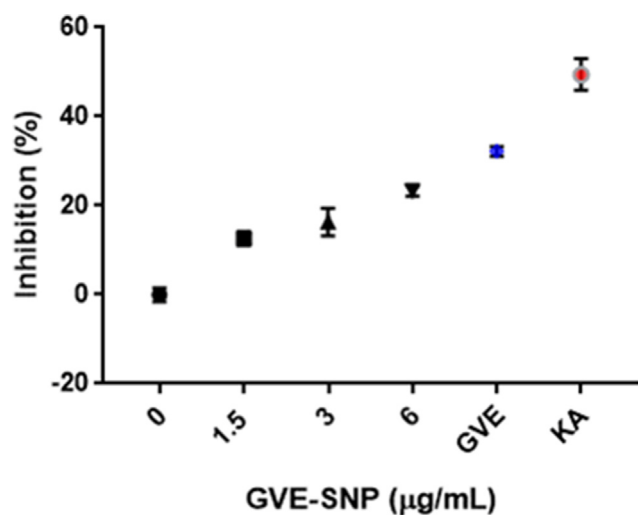
Fig. 7 Tyrosinase inhibitory activity of GVE-SNP.

be attributed to the nanomaterial as opposed to the capping (bio)organic agents. Broadly speaking, the antimicrobial activity of silver nanoparticles is attributable to the released silver ions, which are considered to be the actual biochemically

active agent. The nanoparticles are attracted to the outer membrane surface of the microbes by electrostatic forces. While some of the nanoparticles are taken up intracellularly by the pathogen, others are decomposed into silver ions once in contact with the aqueous micromilieu of the bacterial cell surface. Given its high affinity for sulfur and nitrogen, silver ions interact with various biomolecular components in the cell membrane and organelles including proteins and nucleic acid, causing deleterious structural alteration, damage to the normal functioning of the cells and even cell death. The antimicrobial properties of GVE-SNP suggest that this nanomaterial could be used to abrogate the growth of pernicious bacterial species.

4. Conclusion

This study presents a detail portrait of the biogenic synthesis, optimization and characterization of guava phenolic extract functionalized nanosilver (GVE-SNP). GVE-SNP with desirable physico-chemical attributes was successfully fabricated in a manner that was simple (one-pot at room temperature), fast (within 10 min), eco-friendly (no toxic ingredients) and economical (required only guava phenolic-rich extract). The guava phenolic-rich extract (GVE) used in this study was also prepared free of any noxious chemical reagents. GVE was efficacious as the sole reducing and stabilizing agent during the synthesis of GVE-SNP. Additionally, this investigation highlighted the fact that the prepared GVE-SNP possessed considerable antioxidant, anti-
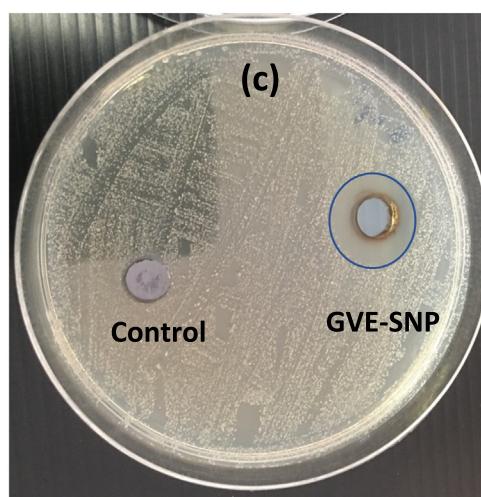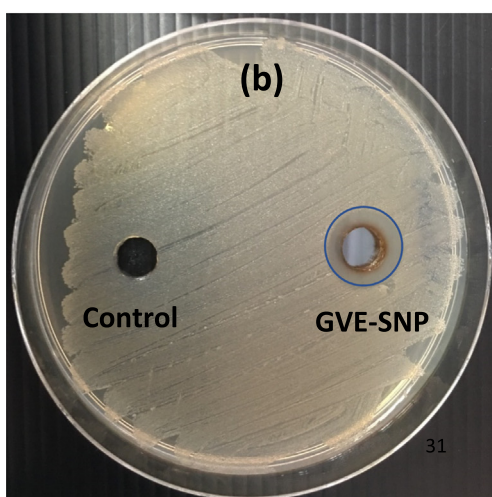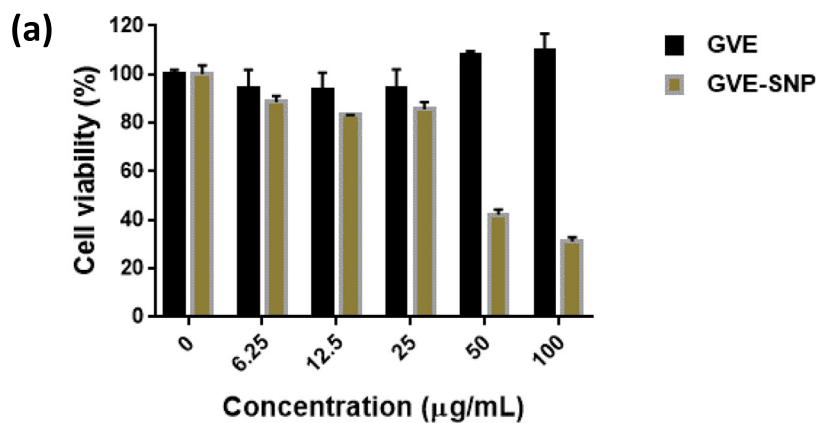

Fig. 8 (a) Cell viability of mouse L929 cells after 24 h treatment with various concentrations of GVE-SNP. The effect of GVE-SNG on the growth of (b) S. aureus and (c) S. epidermidis illustrated by the presence or absence of clear inhibition zones.

tyrosinase, antimicrobial and cytocompatible properties. Taken together, the findings presented in this study reveal a facile, quick, inexpensive, safe and scalable green approach for the reproducible synthesis of biogenic nanosilver based entirely on guava phenolic extract and without requiring any additional chemical reagent, toxic organic solvent or residue. This approach holds promise for the industrial preparation of high quality biogenic nanosilver that could be applied in biological, agricultural and environmental fields.

CRediT authorship contribution statement

Fredrick Nwude Eze: Conceptualization, Methodology, Formal analysis, Investigation, Data curation, Writing – original draft, Writing – review & editing, Supervision, Project administration. **Chitchamai Ovatlarnporn:** Conceptualization, Methodology, Resources, Writing – review & editing, Supervision, Project administration, Funding acquisition. **Sirinporn Nalinbenjapun:** Formal analysis, Investigation, Data curation. **Sasikarn Sripetthong:** Formal analysis, Investigation, Data curation.

Declaration of Competing Interest

The authors declare that they have no known competing financial interests or personal relationships that could have appeared to influence the work reported in this paper.

Acknowledgements

Appendix A. Supplementary material

Supplementary data to this article can be found online at https://doi.org/10.1016/j.arabjc.2022.104167.

References

M. Barbalho, S., Barbalho, S.M., Machado, F.M.V.F., 2012. Psidium Guajava (Guava): A Plant of Multipurpose Medicinal Applications. Medicinal & Aromatic Plants 01.

Bhutto, A.A., Kalay, Ş., Sherazi, S.T.H., Culha, M., 2018. Quantitative structure–activity relationship between antioxidant capacity of phenolic compounds and the plasmonic properties of silver nanoparticles. Talanta 189, 174–181. https://doi.org/10.1016/j.talanta.2018.06.080.

Biswas, B., Rogers, K., McLaughlin, F., Daniels, D., Yadav, A., 2013. Antimicrobial Activities of Leaf Extracts of Guava (Psidium guajava L.) on Two Gram-Negative and Gram-Positive Bacteria. Int J Microbiol, 746165. https://doi.org/10.1155/2013/746165.

Brasiunas, B., Popov, A., Ramanavicius, A., Ramanaviciene, A., 2021. Gold nanoparticle based colorimetric sensing strategy for the determination of reducing sugars. Food Chem. 351, 129238. https://doi.org/10.1016/j.foodchem.2021.129238.

Cervantes, B., Arana, L., Murillo-Cuesta, S., Bruno, M., Alkorta, I., Varela-Nieto, I., 2019. Solid Lipid Nanoparticles Loaded with Glucocorticoids Protect Auditory Cells from Cisplatin-Induced Ototoxicity. J. Clin. Med. 8, 1464. https://doi.org/10.3390/jcm8091464.

Chernousova, S., Epple, M., 2013. Silver as Antibacterial Agent: Ion, Nanoparticle, and Metal. Angew. Chem. Int. Ed. 52, 1636–1653. https://doi.org/10.1002/anie.201205923.

Costa, C., Conte, A., Buonocore, G.G., Lavorgna, M., Del Nobile, M. A., 2012. Calcium-alginate coating loaded with silver-montmorillonite nanoparticles to prolong the shelf-life of fresh-cut carrots. Food Res. Int. 48, 164–169. https://doi.org/10.1016/j.foodres.2012.03.001.

Costa, P.R. da, 2012. Synthesis and characterization of gold nanoparticles as diagnostic and therapeutic tool; Sintese e caracterizacao de nanoparticulas de ouro como ferramenta terapeutica e diagnostica.

Das, G., Patra, J.K., Debnath, T., Ansari, A., Shin, H.-S., 2019. Investigation of antioxidant, antibacterial, antidiabetic, and cytotoxicity potential of silver nanoparticles synthesized using the outer peel extract of Ananas comosus (L.). PLoS ONE 14, e0220950.

Detsri, E., Seeharaj, P., Sriwong, C., 2018. A sensitive and selective colorimetric sensor for reduced glutathione detection based on silver triangular nanoplates conjugated with gallic acid. Colloids Surf., A 541, 36–42. https://doi.org/10.1016/j.colsurfa.2018.01.016.

Díaz-de-Cerio, E., Gómez-Caravaca, A.M., Verardo, V., Fernández-Gutiérrez, A., Segura-Carretero, A., 2016. Determination of guava (Psidium guajava L.) leaf phenolic compounds using HPLC-DAD-QTOF-MS. J. Funct. Foods 22, 376–388. https://doi.org/10.1016/j.jff.2016.01.040.

Eze, F.N., Jayeoye, T.J., Tola, A.J., 2021. Fabrication of label-free and eco-friendly ROS optical sensor with potent antioxidant properties for sensitive hydrogen peroxide detection in human plasma. Colloids Surf., B 204, 111798. https://doi.org/10.1016/j.colsurfb.2021.111798.

Eze, F.N., Nwabor, O.F., 2020. Valorization of Pichia spent medium via one-pot synthesis of biocompatible silver nanoparticles with potent antioxidant, antimicrobial, tyrosinase inhibitory and reusable catalytic activities. Mater. Sci. Eng., C 115, 111104. https://doi.org/10.1016/j.msec.2020.111104.

Eze, F.N., Tola, A.J., Nwabor, O.F., Jayeoye, T.J., 2019. Centella asiatica phenolic extract-mediated bio-fabrication of silver nanoparticles: characterization, reduction of industrially relevant dyes in water and antimicrobial activities against foodborne pathogens. RSC Adv. 9, 37957–37970. https://doi.org/10.1039/C9RA08618H.

Gubitosa, J., Rizzi, V., Fini, P., Del Sole, R., Lopedota, A., Laquintana, V., Denora, N., Agostiano, A., Cosma, P., 2020. Multifunctional green synthetized gold nanoparticles/chitosan/ellagic acid self-assembly: Antioxidant, sun filter and tyrosinase-inhibitor properties. Mater. Sci. Eng., C 106, 110170. https://doi.org/10.1016/j.msec.2019.110170.

He, H., Cai, R., Wang, Y., Tao, G., Guo, P., Zuo, H., Chen, L., Liu, X., Zhao, P., Xia, Q., 2017. Preparation and characterization of silk sericin/PVA blend film with silver nanoparticles for potential antimicrobial application. Int. J. Biol. Macromol. 104, 457–464. https://doi.org/10.1016/j.ijbiomac.2017.06.009.

Iravani, S., Korbekandi, H., Mirmohammadi, S.V., Zolfaghari, B., 2014. Synthesis of silver nanoparticles: chemical, physical and biological methods. Res Pharm Sci 9, 385–406.

Jamkhande, P.G., Ghule, N.W., Bamer, A.H., Kalaskar, M.G., 2019. Metal nanoparticles synthesis: An overview on methods of preparation, advantages and disadvantages, and applications. J. Drug Delivery Sci. Technol. 53, 101174. https://doi.org/10.1016/j.jddst.2019.101174.

Jayeoye, T.J., Eze, F.N., Olatunde, O.O., Benjakul, S., Rujiralai, T., 2021. Synthesis of silver and silver@zero valent iron nanoparticles using Chromolaena odorata phenolic extract for antibacterial activity and hydrogen peroxide detection. J. Environ. Chem. Eng. 9, 105224. https://doi.org/10.1016/j.jece.2021.105224.

Jiménez, Z., Kim, Y.-J., Mathiyalagan, R., Seo, K.-H., Mohanan, P., Ahn, J.-C., Kim, Y.-J., Yang, D.-C., 2018. Assessment of radical scavenging, whitening and moisture retention activities of Panax ginseng berry mediated gold nanoparticles as safe and efficient novel cosmetic material. Artif Cells Nanomed. Biotechnol. 46, 333–340. https://doi.org/10.1080/21691401.2017.1307216.

Jurasekova, Z., Domingo, C., Garcia-Ramos, J.V., Sanchez-Cortes, S., 2014. Effect of pH on the chemical modification of quercetin and structurally related flavonoids characterized by optical (UV-visible and Raman) spectroscopy. Phys. Chem. Chem. Phys. 16, 12802–12811. https://doi.org/10.1039/C4CP00864B.

Kedi, P.B.E., Meva, F.E., Kotsedi, L., Nguemfo, E.L., Zangueu, C.B., Ntoumba, A.A., Mohamed, H.E.A., Dongmo, A.B., Maaza, M., 2018. Eco-friendly synthesis, characterization, in vitro and in vivo anti-inflammatory activity of silver nanoparticle-mediated Selaginella myosurus aqueous extract. Int. J. Nanomed. 13, 8537–8548. https://doi.org/10.2147/IJN.S174530.

Lorena, C., Ressaissi, A., Serralheiro, M.L., 2022. Bioactives from Psidium guajava leaf decoction: LC-HRMS-MS-Qtof identification, bioactivities and bioavailability evaluation. Food Chem. Adv. 1, 100003. https://doi.org/10.1016/j.focha.2021.100003.

Nath, S., Shyanti, R.K., Pathak, B., 2020. Plant-Mediated Synthesis of Silver and Gold Nanoparticles for Antibacterial and Anticancer Applications. In: Patra, J.K., Fraceto, L.F., Das, G., Campos, E.V. R. (Eds.), Green Nanoparticles: Synthesis and Biomedical Applications, Nanotechnology in the Life Sciences. Springer International Publishing, Cham, pp. 163–186. https://doi.org/10.1007/978-3-030-39246-8_7.

Navarro, J.R.G., Werts, M.H.V., 2012. Resonant light scattering spectroscopy of gold, silver and gold–silver alloy nanoparticles and optical detection in microfluidic channels. Analyst 138, 583–592. https://doi.org/10.1039/C2AN36135C.

Nguyen, D.H., Vo, T.N.N., Nguyen, N.T., Ching, Y.C., Thi, T.T.H., 2020. Comparison of biogenic silver nanoparticles formed by Momordica charantia and Psidium guajava leaf extract and antifungal evaluation. PLoS ONE 15, e0239360.

Ntoumba, A.A., Meva, F.E., Ekoko, W.E., Foko, L.P.K., Hondt, E.N., Schlüsener, C., Moll, B., Loe, G.E., Kedi, P.B.E., Fouda, J.Y.S., Janiak, C., Lehman, L.G., 2019. Biogenic Synthesis of Silver Nanoparticles Using Guava (Psidium guajava) Leaf Extract and Its Larvicidal Action against Anopheles gambiae. J. Biomater. Nanobiotechnol. 11, 49–66. https://doi.org/10.4236/jbnb.2020.111004.

Padilla-Cruz, A.L., Garza-Cervantes, J.A., Vasto-Anzaldo, X.G., García-Rivas, G., León-Buitimea, A., Morones-Ramírez, J.R., 2021. Synthesis and design of Ag–Fe bimetallic nanoparticles as antimicrobial synergistic combination therapies against clinically relevant pathogens. Sci. Rep. 11, 5351. https://doi.org/10.1038/s41598-021-84768-8.

Paramelle, D., Sadovoy, A., Gorelik, S., Free, P., Hobley, J., Fernig, D.G., 2014. A rapid method to estimate the concentration of citrate capped silver nanoparticles from UV-visible light spectra. Analyst 139, 4855–4861. https://doi.org/10.1039/C4AN00978A.

R. Pompeu, D., Larondelle, Y., Rogez, H., Abbas, O., Fernández Pierna, J.A., Baeten, V., 2018. Characterization and discrimination of phenolic compounds using Fourier transform Raman spectroscopy and chemometric tools. Biotechnol. Agron. Soc Environ. https://doi.org/10.25518/1780-4507.16270.

Qiao, L., Sun, Y., Chen, R., Fu, Y., Zhang, W., Li, X., Chen, J., Shen, Y., Ye, X., 2014. Sonochemical Effects on 14 Flavonoids Common in Citrus: Relation to Stability. PLoS ONE 9, e87766.

Raghunandan, D., Mahesh, B.D., Basavaraja, S., Balaji, S.D., Manjunath, S.Y., Venkataraman, A., 2011. Microwave-assisted rapid extracellular synthesis of stable bio-functionalized silver nanoparticles from guava (Psidium guajava) leaf extract. J. Nanopart. Res. 13, 2021–2028.

Rahman, M.M., Zaman, S., Mamun, F., Gias, Z.T., Alam, M.N., Ulla, A., Hossain, M.H., Reza, H.M., Alam, M.A., 2018. Phenolic content analysis in Psidium guajava leaves powder by HPLC-DAD system and in vivo renoprotective and antioxidant activities in fludrocortisone acetate-induced rats. J. Food Biochem. 42, e12687.

Rehana, D., Mahendiran, D., Kumar, R.S., Rahiman, A.K., 2017. Evaluation of antioxidant and anticancer activity of copper oxide nanoparticles synthesized using medicinally important plant extracts. Biomed. Pharmacother. 89, 1067–1077. https://doi.org/10.1016/j.biopha.2017.02.101.

Ruseva, V., Lyons, M., Powell, J., Austin, J., Malm, A., Corbett, J., 2018. Capillary dynamic light scattering: Continuous hydrodynamic particle size from the nano to the micro-scale. Colloids Surf., A 558, 504–511. https://doi.org/10.1016/j.colsurfa.2018.09.022.

Sandhir, R., Yadav, A., Sunkaria, A., Singhal, N., 2015. Nano-antioxidants: An emerging strategy for intervention against neurodegenerative conditions. Neurochem Int 89, 209–226. https://doi.org/10.1016/j.neuint.2015.08.011.

Selvaraj, R., Pai, S., Murugesan, G., Pandey, S., Bhole, R., Gonsalves, D., Varadavenkatesan, T., Vinayagam, R., 2021. Green synthesis of magnetic α–Fe2O3 nanospheres using Bridelia retusa leaf extract for Fenton-like degradation of crystal violet dye. Appl Nanosci 11, 2227–2234. https://doi.org/10.1007/s13204-021-01952-y.

Singh, S., Chunglok, W., Nwabor, O.F., Ushir, Y.V., Singh, S., Panpipat, W., 2021. Hydrophilic Biopolymer Matrix Antibacterial Peel-off Facial Mask Functionalized with Biogenic Nanostructured Material for Cosmeceutical Applications. J. Polym. Environ. https://doi.org/10.1007/s10924-021-02249-5.

Sougandhi, P.R., Ramanaiah, S., 2020. Green synthesis and spectral characterization of silver nanoparticles from Psidium guajava leaf extract. Inorganic Nano-Metal Chem. 50, 1290–1294. https://doi.org/10.1080/24701556.2020.1745839.

Sugumaran, M., Barek, H., 2016. Critical Analysis of the Melanogenic Pathway in Insects and Higher Animals. Int. J. Mol. Sci. 17, 1753. https://doi.org/10.3390/ijms17101753.

Tao, G., Cai, R., Wang, Y., Liu, L., Zuo, H., Zhao, P., Umar, A., Mao, C., Xia, Q., He, H., 2019a. Bioinspired design of AgNPs embedded silk sericin-based sponges for efficiently combating bacteria and promoting wound healing. Mater. Des. 180, 107940. https://doi.org/10.1016/j.matdes.2019.107940.

Tao, G., Wang, Y., Cai, R., Chang, H., Song, K., Zuo, H., Zhao, P., Xia, Q., He, H., 2019b. Design and performance of sericin/poly (vinyl alcohol) hydrogel as a drug delivery carrier for potential wound dressing application. Mater. Sci. Eng., C 101, 341–351. https://doi.org/10.1016/j.msec.2019.03.111.

Tao, G., Cai, R., Wang, Y., Zuo, H., He, H., 2021. Fabrication of antibacterial sericin based hydrogel as an injectable and mouldable wound dressing. Mater. Sci. Eng., C 119, 111597. https://doi.org/10.1016/j.msec.2020.111597.

Thanh, N.T.K., Maclean, N., Mahiddine, S., 2014. Mechanisms of Nucleation and Growth of Nanoparticles in Solution. Chem. Rev. 114, 7610–7630. https://doi.org/10.1021/cr400544s.

Thomä, S.L.J., Krauss, S.W., Eckardt, M., Chater, P., Zobel, M., 2019. Atomic insight into hydration shells around facetted nanoparticles. Nat Commun 10, 995. https://doi.org/10.1038/s41467-019-09007-1.

Ulaeto, S.B., Mathew, G.M., Pancrecious, J.K., Nair, J.B., Rajan, T.P. D., Maiti, K.K., Pai, B.C., 2020. Biogenic Ag Nanoparticles from Neem Extract: Their Structural Evaluation and Antimicrobial Effects against Pseudomonas nitroreducens and Aspergillus unguis (NII 08123). ACS Biomater. Sci. Eng. 6, 235–245. https://doi.org/10.1021/acsbiomaterials.9b01257.

Varadavenkatesan, T., Selvaraj, R., Vinayagam, R., 2020. Green synthesis of silver nanoparticles using Thunbergia grandiflora flower extract and its catalytic action in reduction of Congo red dye. Materials Today: Proceedings, Advanced Materials for Clean Energy and Health Applications (AMCEHA), University of Jaffna, Jafna, Sri Lanka, 6-8 February, 2019 23, pp. 39–42. https://doi.org/10.1016/j.matpr.2019.05.441.

Varadavenkatesan, T., Pai, S., Vinayagam, R., Selvaraj, R., 2021. Characterization of silver nano-spheres synthesized using the extract of Arachis hypogaea nuts and their catalytic potential to degrade dyes. Mater. Chem. Phys. 272, 125017. https://doi.org/10.1016/j.matchemphys.2021.125017.

Venugopal, G., 2017. Green synthesis of silver nanoparticles from Psidium guajava leaves and its antibacterial activity. IJB 6, 5441. https://doi.org/10.21746/ijbio.2017.07.003.

Vinayagam, R., Varadavenkatesan, T., Selvaraj, R., 2018. Green synthesis, structural characterization, and catalytic activity of silver nanoparticles stabilized with Bridelia retusa leaf extract. Green Process. Synth, 7, 30–37. https://doi.org/10.1515/gps-2016-0236.

Wang, L., Xie, J., Huang, T., Ma, Y., Wu, Z., 2017. Characterization of silver nanoparticles biosynthesized using crude polysaccharides of Psidium guajava L. leaf and their bioactivities. Materials Letters, 35th Anniversary of. Mater. Lett. 208, 126–129. https://doi.org/10.1016/j.matlet.2017.05.014.

Wang, L., Lu, F., Liu, Y., Wu, Y., Wu, Z., 2018a. Photocatalytic degradation of organic dyes and antimicrobial activity of silver nanoparticles fast synthesized by flavonoids fraction of Psidium guajava L. leaves. J. Mol. Liq. 263, 187–192. https://doi.org/10.1016/j.molliq.2018.04.151.

Wang, L., Wu, Y., Xie, J., Wu, S., Wu, Z., 2018b. Characterization, antioxidant and antimicrobial activities of green synthesized silver nanoparticles from Psidium guajava L. leaf aqueous extracts. Mater. Sci. Eng., C 86, 1–8. https://doi.org/10.1016/j.msec.2018.01.003.

Xia, Y., Xiong, Y., Lim, B., Skrabalak, S.E., 2009. Shape-controlled synthesis of metal nanocrystals: simple chemistry meets complex physics? Angew. Chem. Int. Ed. Engl. 48, 60–103. https://doi.org/10.1002/anie.200802248.

Yoosaf, K., Ipe, B.I., Suresh, C.H., Thomas, K.G., 2007. In Situ Synthesis of Metal Nanoparticles and Selective Naked-Eye Detection of Lead Ions from Aqueous Media. J. Phys. Chem. C 111, 12839–12847. https://doi.org/10.1021/jp073923q.

You, D.-H., Park, J.-W., Yuk, H.-G., Lee, S.-C., 2011. Antioxidant and tyrosinase inhibitory activities of different parts of guava (Psidium guajava L.). Food Sci. Biotechnol. 20, 1095. https://doi.org/10.1007/s10068-011-0148-9.

Zhao, T., Sun, R., Yu, S., Zhang, Z., Zhou, L., Huang, H., Du, R., 2010. Size-controlled preparation of silver nanoparticles by a modified polyol method. Colloids Surf., A 366, 197–202. https://doi.org/10.1016/j.colsurfa.2010.06.005.